The Regional Analysis System for the Operational "Early" Eta Model: Original 80-km Configuration and Recent Changes

ERIC ROGERS, DENNIS G. DEAVEN AND GEOFFREY J. DIMEGO

Development Division, National Centers for Environmental Prediction, NWS/NOAA, Washington, D.C.

ABSTRACT

The analysis component of the National Centers for Environmental Prediction (NCEP) operational "early" 80-km eta model, as implemented in July 1993, is described. This optimum interpolation (OI) analysis is fully multivariate for wind and geopotential height (univariate for specific humidity) and is performed directly on the eta model's vertical coordinate. Although the eta OI analysis and model performance has been generally favorable when compared to the Limited-Area Fine Mesh Model (LFM) and the Nested Grid Model (NGM), deficiencies in the eta OI analysis fields have been observed, especially near the surface.

A series of improvements to the eta OI analysis is described. A refinement to the eta model orography, which created a more realistic depiction of the model terrain, is also discussed along with the impact of these changes on analysis and model performance. These changes were implemented in the early eta system in September 1994.

The operational configuration of the new mesoscale (29 km) eta model system is introduced, consisting of a mesoscale eta-based data assimilation system (EDAS) and the mesoscale forecast. An example of an analysis produced by the mesoscale EDAS is presented for comparison with the operational 80-km eta OI analysis. A brief description of more recent changes to the early eta system are also described.

1. Introduction

The primary effort in regional and mesoscale modeling at the National Centers for Environmental Prediction (NCEP) is focused on the development of the eta model. The initial work at the NCEP concentrated on extensive testing of the eta model at 80-km horizontal resolution to refine model physics. The culmination of this effort was the implementation of a synoptic-scale version of the eta model with 80-km horizontal resolution and 38 vertical layers in June 1993, replacing the Limited Area Fine-mesh Model (LFM) in providing early forecast guidance over North America (Black et al. 1993). The so-called "early" eta model run uses initial conditions obtained from a regional optimum interpolation (ROI) analysis done on the eta vertical coordinate, using a 6-h forecast of the NCEP global spectral model from the Global Data Assimilation System (GDAS: Kanamitsu et al. 1991) as a first guess, with boundary conditions obtained from the previous aviation run of the NCEP global spectral model.

This paper describes the ROI analysis package as used in the operational early eta system from June 1993–June 1995. A brief description of the eta model

Corresponding author address: Dr. Eric Rogers, National Centers for Environmental Prediction, W/NMC22, World Weather Building, Room 204, Washington, DC 20233.

is given in section 2 and the original analysis system implemented in June 1993 will be described in section 3. Results from the original system are shown in section 4, and changes prompted by these findings implemented in September 1994 will be discussed in section 5. A discussion of an intermittent eta-based data assimilation system follows in section 6. A brief description of more recent changes to the early eta system implemented in September 1995 is given in section 7.

2. Eta model description

The eta coordinate as defined by Mesinger (1984) is a generalization of the terrain-following sigma coordinate. Although both sigma and eta coordinates are pressure-based and normalized from 0 to 1, eta is normalized with respect to sea level pressure instead of the surface pressure normalization used in the sigma framework. The resultant eta surfaces tend to be quasi-horizontal, thus eliminating errors in the pressure gradient force computation over steeply sloped terrain in sigma coordinates (Mesinger and Black 1992). A consequence of the eta model vertical structure is that the model orography is configured in the shape of discrete steps. As seen in Fig. 1, the top of each step coincides exactly with a model interface. The step mountains are computed based on the "silhouette" orography method (Mesinger and Collins 1987) so that their heights are maximized based upon the input 10-min surface elevation data (Joseph 1980).
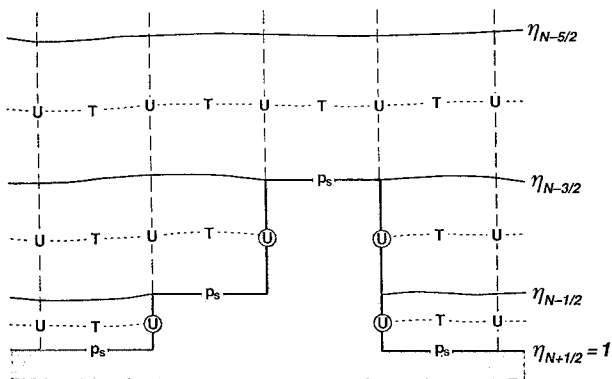
FIG. 1. Idealized vertical cross section of the eta model's step mountains. Here "T" indicates a mass variable within each grid box, while "U" represents both horizontal wind components. The circled "U" on the sides of the steps indicate points at which the horizontal wind components are set to zero at all times. Term p_s is the surface pressure.
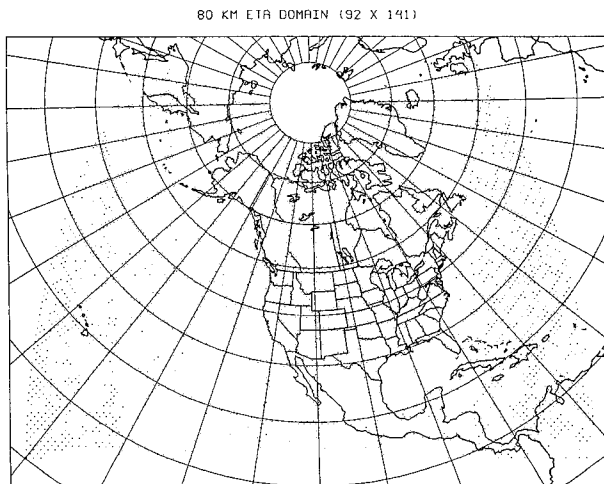

FIG. 2. The horizontal area and grid points of the operational 80-km eta model grid.

The horizontal domain of the operational 80-km eta model grid is shown in Fig. 2. The eta model employs a semistaggered Arakawa e-grid (Arakawa and Lamb 1977) in which wind points are adjacent to mass points, as depicted in Fig. 1. The eta model grid is configured in a rotated latitude–longitude framework. This co-ordinate system is created by rotating the earth's entire geographic latitude–longitude grid so that the intersection of the equator and the prime meridian is placed over the center of the forecast area. Each grid box consists of a mass point surrounded by four velocity points, all of which lie along parallels of rotated latitude–longitude.

Table 1 summarizes model numerics and physics for the operational 80-km configuration. Specific details on eta model dynamics and physical parameterizations can be found in Black (1988, 1994), Janjic (1990, 1994), Mesinger et al. (1988), and Gerrity et al. (1994).

3. Regional eta OI analysis—June 1993 version

The method used to provide initial conditions to the early eta run is a generalization of the ROI analysis (DiMego 1988) used in the original configuration of the Regional Analysis and Forecast System (RAFS: Hoke et al. 1989). Initially, a first guess at 0000 or 1200 UTC is provided by a 6-h forecast from the GDAS. The 6-h forecast spectral coefficients (currently T126 resolution, 28 sigma layers) are transformed onto a latitude–longitude grid whose domain covers the 80-km eta model grid depicted in Fig. 2. This grid contains 295 × 120 grid points with a horizontal resolution of 0.75° latitude–longitude. Such resolution is much greater than the observational density over oceanic and polar regions. Thus, to reduce computing costs, the ROI analysis is performed on a thinned grid, for which

the resolution remains 0.75° over the contiguous United States but is increased to about 2.0° elsewhere. To minimize surface pressure errors and inconsistencies between the global spectral model terrain (which is also derived from the 10-min surface elevation data used by the eta model) and the step mountains, the orography on the analysis grid is precomputed using the discretization procedure described in section 2a. After the spectral to grid transformation, the GDAS forecast is vertically interpolated to the eta model layers.

The procedure for processing observations for ingestion into the early eta ROI analysis is identical to the process described by DiMego (1988) for the RAFS, except that the time window for data acceptance for the early eta analysis is 45 min earlier (2100–0115 UTC for the 0000 UTC analysis, 0900–1315 UTC for the

TABLE 1. 80-km eta model numerics–physics.

Numerics
• 80-km horizontal resolution, 38 vertical layers, pressure at model top = 50 mb
• Fundamental model time step = 200 s
• Semistaggered Arakawa e-grid
• Silhouette orography in step mountain form
• Split-explicit time differencing scheme

| Physics |
| --- |
| • Modified Betts–Miller (1986) convective adjustment scheme for deep and shallow convection |
| • Mellor–Yamada (1974, 1982) level 2.5 model for free atmosphere vertical turbulent exchange; Mellor–Yamada level 2.0 model near ground |
| • GFDL radiation scheme: Lacis and Hanson (1974) (short wave); Fels and Schwarztkopf (1975) (long wave) |
| • Viscous sublayer over water (Liu et al. 1979; Mangarella et al. 1973) |
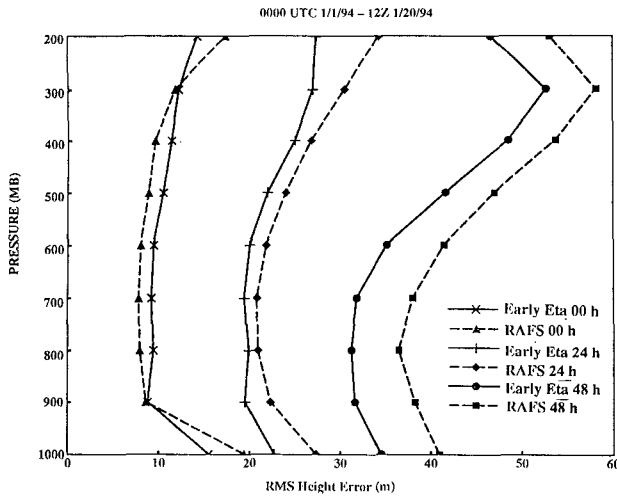
FIG. 3. Grid to rawinsonde root-mean-square errors for the 00-, 24-, and 48-h early eta and RAFS forecasts of geopotential height for the period 1–20 January 1994.

1200 UTC analysis) than that for the RAFS. The impact of the earlier cutoff time on the observation counts (not shown) is small, manifested by less rawinsonde data above 100 mb and 10%–20% less aircraft data, primarily outside the United States. All available multilevel (rawinsondes, wind profilers, etc.) and surface observations are used. After all data preprocessing is

completed, rawinsonde height and temperature data are subjected to "complex" hydrostatic quality control (Collins and Gandin 1992; Gandin et al. 1993).

After the GDAS first guess is transformed from spectral to grid space, it is interpolated to each observation location. This interpolation is quadratic in ln p for heights and linear in ln p for wind and specific humidity. The observed increments are then computed (observation minus first guess); this quantity represents the observed correction to the first guess. The observed increments are then passed to an optimum interpolation-based data quality control (OIQC) algorithm (Woollen 1991). The OIQC acts to remove obviously erroneous observations that are the result of instrumental, human, or communications errors and to remove unrepresentative reports that may be meteorologically correct but depict scales that are not resolvable by the analysis–forecast system.

Following the OIQC algorithm, the ROI analysis of the observed increments is performed on the analysis grid. This analysis is basically the system described by DiMego (1988), except that the analysis is performed on the eta vertical coordinate. The analysis is multivariate in geopotential height and wind and univariate in specific humidity. A preliminary univariate 1000-mb height analysis is performed, from which temperature profiles from polar-orbiting satellites are processed into profiles of geopotential thickness. The geostrophic coupling of height and wind increments is
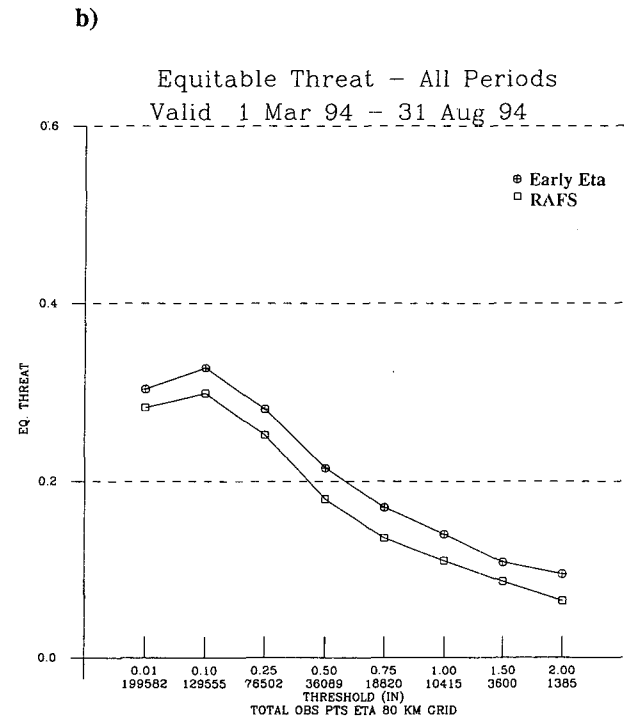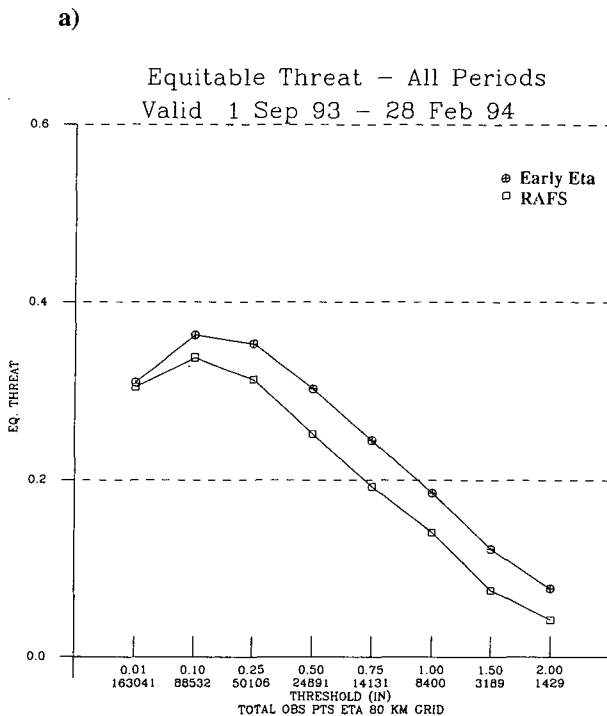
a)

b)

FIG. 4. Equitable threat skill scores for precipitation forecasts (all periods) of the early eta model and Nested Grid Model (RAFS) for (a) September 1993–February 1994 and (b) March–August 1994.

a)

Bias sum of all forecasts
Valid 1 Sep 93 – 28 Feb 94

b)

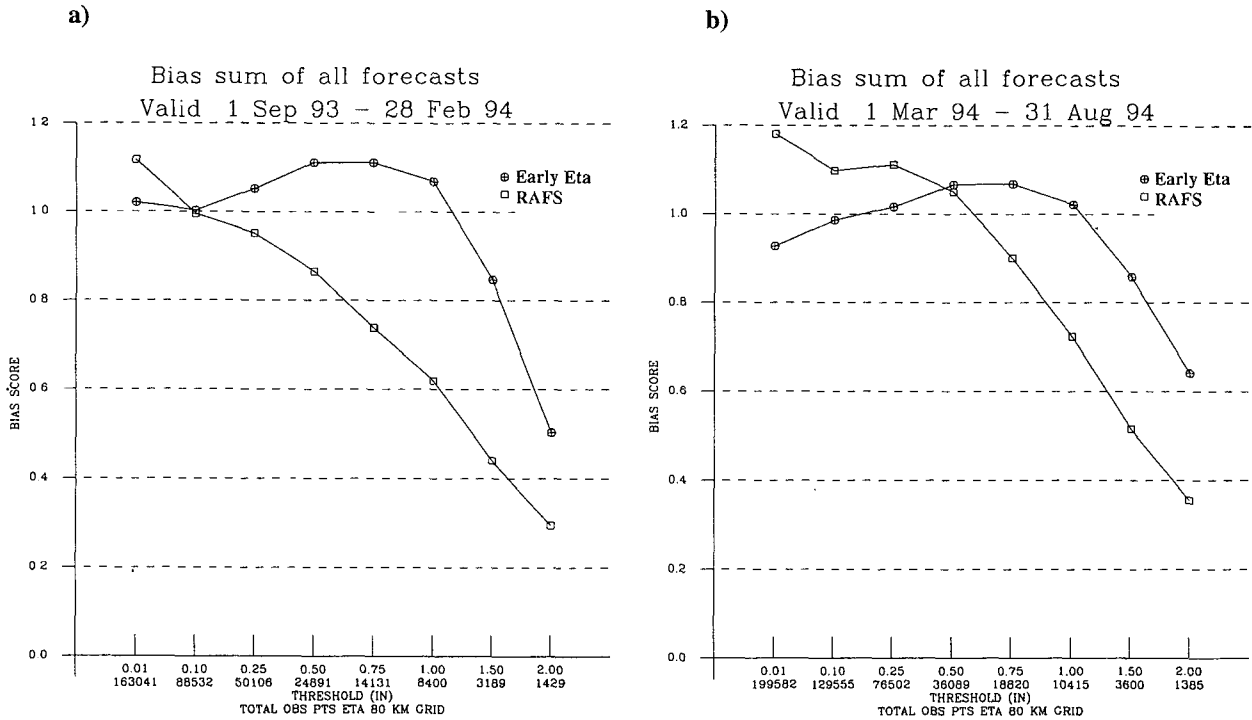Bias sum of all forecasts
Valid 1 Mar 94 – 31 Aug 94

FIG. 5. Same as Fig. 4 but for bias scores.

relaxed in the lower layers to account for ageostrophic frictional effects near the surface. Up to 30 geopotential height and/or wind observed increments within a three dimensional volume around an analysis grid point are chosen to compute the correction to the first guess, of which up to 20 are obtained from multilevel data and the remaining amount allocated to single-level observations. Thus, the analyzed value of z, u, or v is the sum of the first guess and a summation of the weighted corrections to the first guess based on the observed increments. The ROI analysis produces consistent height corrections at the top and bottom of each layer by forcing the data selection at the top and bottom to be the same (DiMego et al. 1992). This procedure acts to reduce noise in the temperature field derived from the ROI analysis.

For the univariate moisture analysis, up to 10 specific humidity increments within the grid volume are chosen. Anisotropic weighting of the moisture increments is done, dependent on the wind speed, wind direction, and vertical stability. After all analysis corrections are computed, the analysis fields on the thinned grid are interpolated back to the full analysis grid and then added to the first guess.

4. Performance of the early eta system

a. Early eta versus LFM

Black et al. (1993) provided a brief description of the eta model and its analysis along with results from

a battery of objective verification scores, a summary of which follows. Forecast performance of the early eta system and the LFM for March 1993 (using the RAFS analysis for verification) was evaluated using the following objective scores: correlation coefficient, S1 score, 12-h tendency correlation and tendency S1 (defined in the appendix) for the parameters of lifted index, relative humidity, height, temperature, wind speed, and vorticity. In an overwhelming majority of cases, the early eta scored higher than the LFM. Forecast versus rawinsonde verifications were computed for a 35-day period in Spring 1993. For verification against rawinsondes, the forecast fields are interpolated bilinearly to the rawinsonde locations, using model fields and observations on mandatory pressure levels. Bias statistics, while generally favoring the early eta over the LFM, also indicated the following: 1000-mb early eta specific humidity forecasts were too high (0.5 g kg^{-1}) and temperatures were too low (1.5°–2.0°C); low-level wind speeds were too strong; mid-level heights were too low—a result of temperatures being too low in the lower troposphere. Jet stream winds were too weak, as usual, but only one-half as much as in the LFM. Standard deviation results for specific humidity, height, temperature, and wind were universally favorable to the early eta system. Root-mean-square (rms) errors at 48-h for the same variables in the early eta were at the same level as the 12-h errors in the LFM—a full day and a half advantage at all levels.
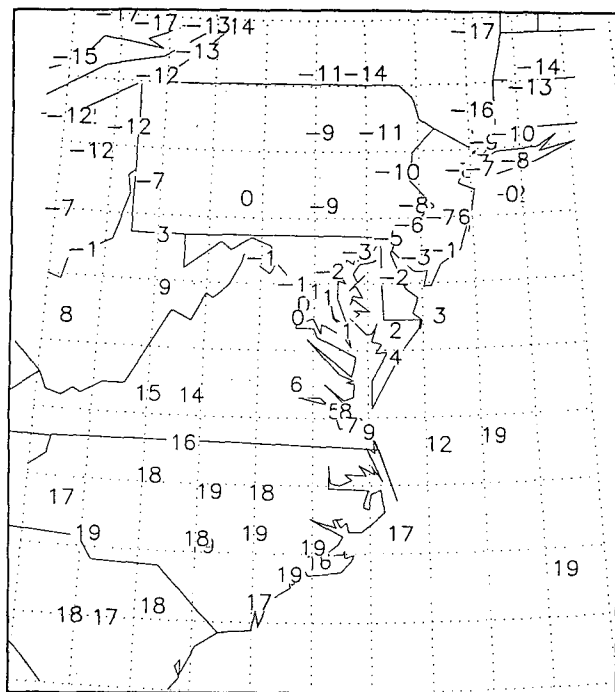
FIG. 6. Observed surface temperatures (°C)
at 1200 UTC 9 February 1994.

Verification of 24-h precipitation amounts showed a clear advantage for the early eta model over the LFM during the warm season. Cold season (March 1993) performance favored the LFM only in the rain–no-rain category—since extremely high biases at the larger amounts were present in the LFM statistics. Overall, the early eta precipitation forecasts have little or no bias in either warm or cold seasons.

b. Early eta versus RAFS

Another measure of eta model performance is the comparison with the Nested Grid Model (NGM), which is the forecast model component of the RAFS. Whereas the early eta was universally superior to the LFM in all categories of comparison to the rawinsonde data, it is not always the clear winner versus the RAFS. Verification of RAFS and early eta geopotential height forecasts against rawinsonde data for 1–20 January 1994 (Fig. 3) reveal that the rms errors of the RAFS analysis was about 20% lower than the early eta analysis throughout most of the troposphere. By 24 hours, the early eta forecast rms errors were smaller than the RAFS errors, a trend that continued through 48 hours. Since the RAFS analysis is the result of a 12-h data assimilation using the NGM with 3-h analysis updates, it takes full advantage of the asynoptic observations over North America, including aircraft and wind profiler data. The first guess for the early eta system is obtained from a 6-h forecast of the coarser horizontal

resolution (T126, approximately 105 km) NCEP global spectral model, produced by the 6-h intermittent GDAS. Thus, the RAFS analysis has some distinct advantages over the early eta analysis. Since the early eta rms height errors were lower than the RAFS scores by 24-h, it is clear that the eta model was able to overcome this initial disadvantage. Such findings have served as an impetus for NMC to develop an eta-based regional data assimilation system, which will be discussed in section 6.

A comparison of the Equitable Threat Score [ETS: called skill-corrected Critical Success Index in Schaefer (1990); defined in the appendix] of 24-h accumulated precipitation for all forecast periods of the early eta and the RAFS for September 1993 to February 1994 and March to August 1994 is presented in Fig. 4. As with the early eta–LFM comparison (Black et al. 1993, not shown), the early eta is superior to the RAFS at all thresholds. The bias scores for the same two periods (Fig. 5) reveal that the RAFS has a steady reduction in bias score with increasing threshold amount. The early eta bias scores for both seasons remained nearer to 1.0 than the RAFS scores at thresholds <1.00 in. These results are consistent with those reported by Mesinger et al. (1995), who state that the use of the eta vertical coordinate and the discretization of the model orography contributes to the ability of the eta model to be more skillful in precipitation forecasting
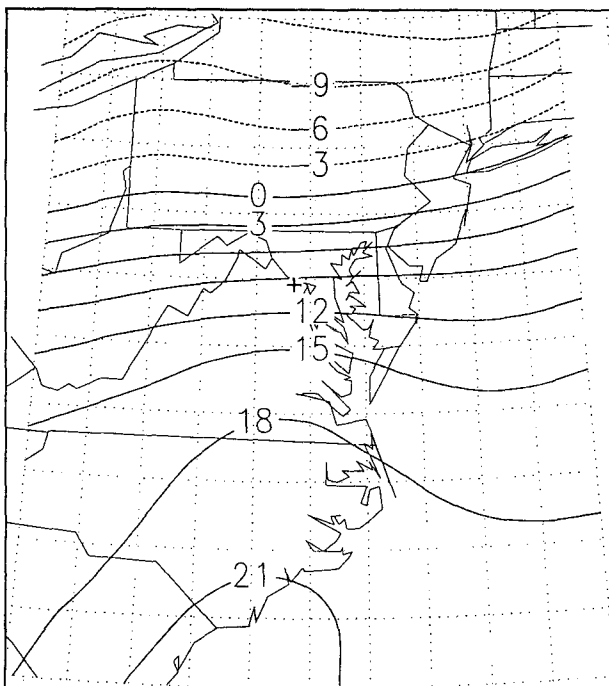

FIG. 7. Post-processed 2-m (shelter) temperature from the early eta analysis valid 1200 UTC 9 February 1994. Contour interval = 3°C. Location of Dulles Airport, Sterling, Virginia (IAD), is noted with a "+".
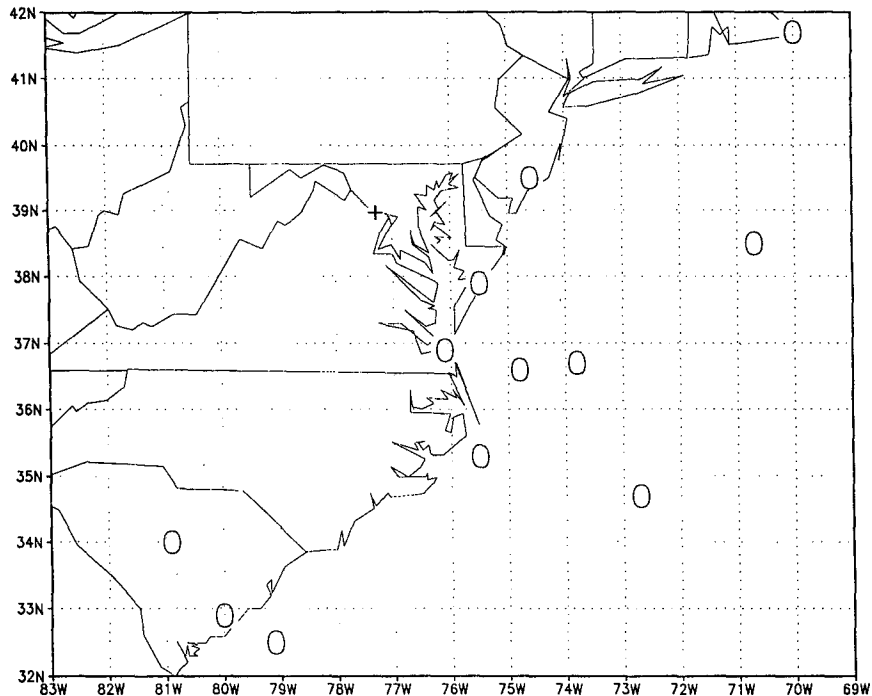
FIG. 8. Location of observations (denoted by the "O") used in the early eta lowest model layer height analysis valid 1200 UTC 9 February 1994.

than the NGM, which uses a sigma coordinate system. To prove this point, Mesinger et al. tested the eta model in "sigma" mode, in which the model was run with a terrain-following sigma coordinate. The sigma eta forecasts produced lower ETS than the early eta, although better ETS than the NGM and the NCEP global spectral model. These results suggest that both the use of step mountains and the eta model physics led to better precipitation forecasts.

c. Analysis example: 1200 UTC 9 February 1994

Forecasters in the NCEP's Meteorological Operations Division, in addition to their assigned duties, frequently provide feedback to NCEP Development Division staff on analysis and model performance. Through this feedback, problems with the early eta analysis were discovered, an example of which is the 1200 UTC 9 February 1994 case. The observed surface temperatures (Fig. 6) depict a typical cold season pattern over the mid-Atlantic states, with cold air dammed up east of the Appalachian mountains over Maryland, eastern Virginia, and Pennsylvania. Warmer air is observed over southwestern Virginia, West Virginia, and southwest Pennsylvania. The post-processed 2-m (shelter) temperature from the early eta analysis (Fig. 7) fails to capture the cool pool of air over central Maryland and Virginia, with analyzed errors up to 10°C.

Further investigation of this case highlighted several deficiencies in the analysis package originally implemented with the early eta system, especially in the use of surface observations. Figure 8 shows the stations chosen by the early eta ROI selection algorithm for the lowest model-layer height analysis at the grid point closest to Dulles Airport, Sterling, Virginia (IAD), which reported a surface temperature of −1°C (Fig. 6). Instead of using IAD and adjacent observations, the selection algorithm in the ROI analysis chose stations primarily in the warmer air to the south and east of IAD. Two obvious problems with the surface analysis and model terrain became apparent.

1) To avoid problems with the update of surface pressure in the ROI analysis, surface observations located below the *model* terrain were excluded from the analysis when it was first implemented. These problems were later fixed, but the surface data switch in the analysis was not changed.

2) The silhouette orography algorithm does not produce terrain that accurately reflects the topography gradient near local maxima. For example, the model grid point closest to IAD, with an elevation of 85 m, was located on the fifth step above sea level, with model elevation of about 270 m. The grid point closest to Washington National Airport (DCA), at 5 m above sea level, was located at the fourth step above sea level, a model elevation of 180 m.

a)   b)

ETA TOPOGRAPHY (OLD, CINT=250)   ETA TOPOGRAPHY (OLD, CINT=100)
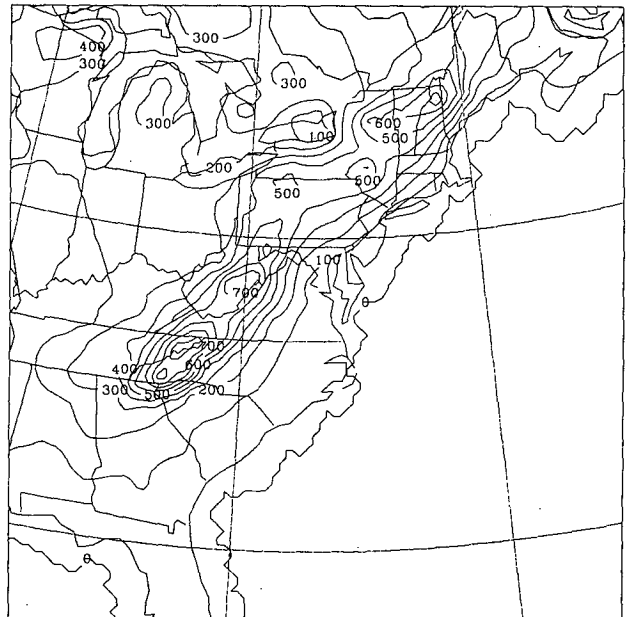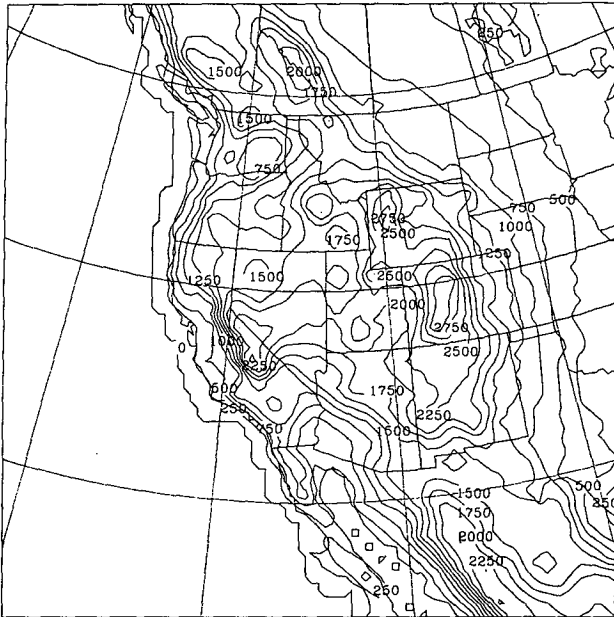
c)   d)

ETA TOPOGRAPHY (OLD-NEW, CINT=50)   ETA TOPOGRAPHY (OLD-NEW, CINT=25)
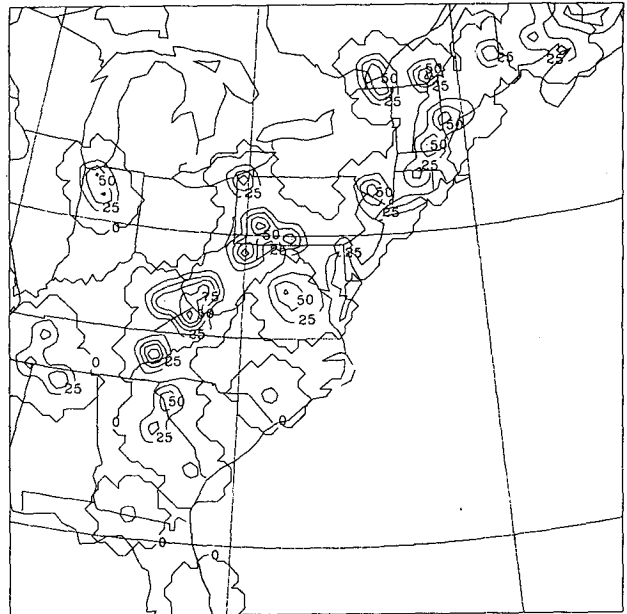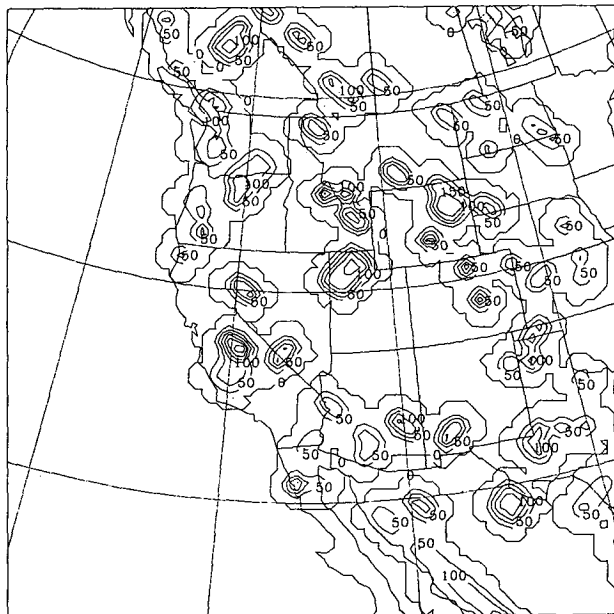
FIG. 9. Surface height (m) from the original 80-km eta model orography (OLD) over (a) the western United States (contour interval = 250 m), and (b) the eastern United States (contour interval = 100 m). Surface height difference between the original silhouette orography and the new silhouette–mean orography (OLD–NEW) over (c) the western United States (contour interval = 50 m), and (d) eastern United States (contour interval = 25 m).
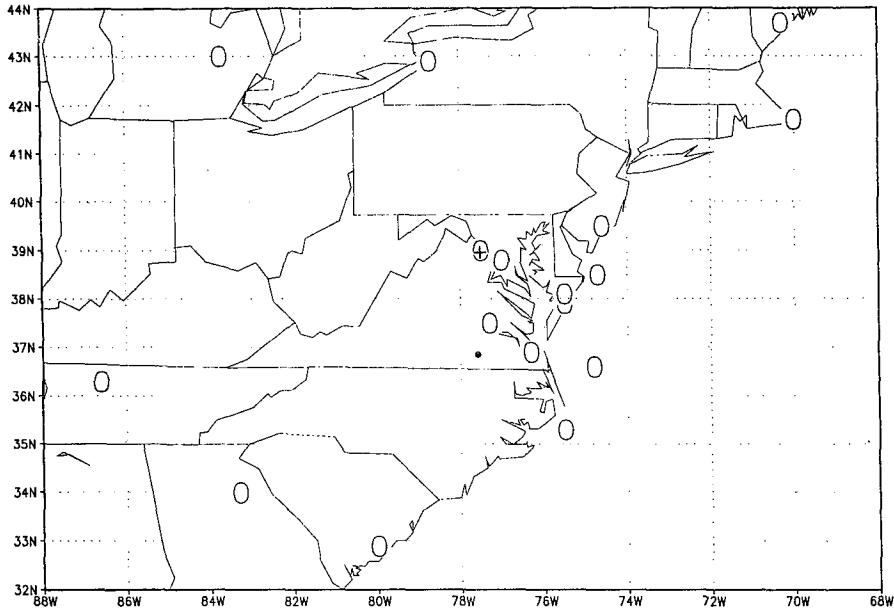
FIG. 10. Same as Fig. 8 but for the ETAY analysis valid 1200
UTC 9 February 1994.

Based on these findings, a series of changes to the eta model orography formulation and to the eta ROI analysis were done. This system, designated internally_ as ETAY, was tested in parallel to the operational early eta system from March–August 1994. Details on these changes and their impact on analysis and model performance are discussed below.

silhouette methodology, but at land points where the observed topography is concave (e.g., a valley) the silhouette elevation is replaced by the average elevation. The impact of this change is to enhance the model surface height gradient in regions adjacent to local

5. Changes to the early eta system—September 1994

a. Orography change

To partially alleviate the terrain problem discussed above, the silhouette mountains were replaced with "silhouette-mean" mountains (Mesinger 1994, personal communication). This method still employs the

TABLE 2. Coefficients that define the width of the horizontal and vertical correlation functions for mass and wind.

Level	Early eta		ETAY	
	$k_h(10^{-6} \text{ km}^{-2})$	k_p	$k_h(10^{-6} \text{ km}^{-2})$	k_p
1	4.065	9	7.391[a]	12
2	4.065	9	6.775[a]	12
3	3.695	9	5.543[a]	12
4	3.325	9	4.927[a]	12
5	3.080	9	4.680[a]	12
6–36	2.956	9	4.435	12
37	2.463	9	2.956	12
38	1.970	9	1.970	12

[a] Applied to the analysis levels 1–5 above ground over entire grid.
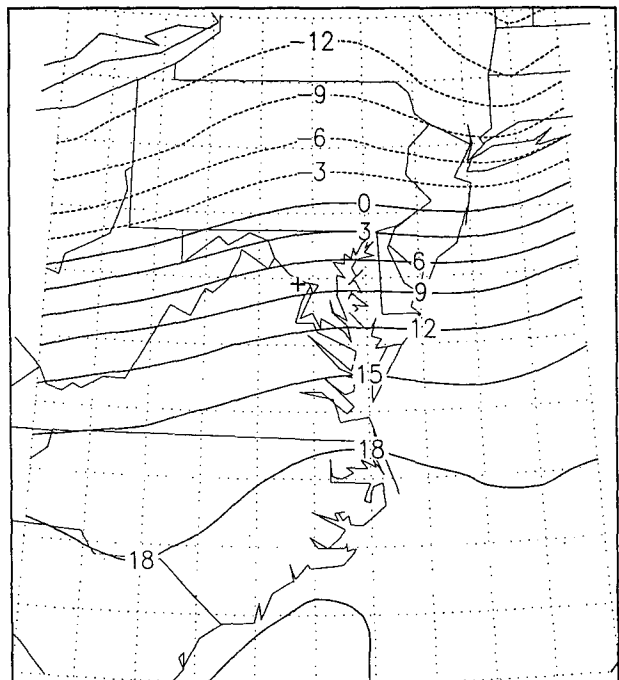

FIG. 11. Same as Fig. 7 but for the ETAY analysis valid 1200
UTC 9 February 1994.

Verification Score Differences
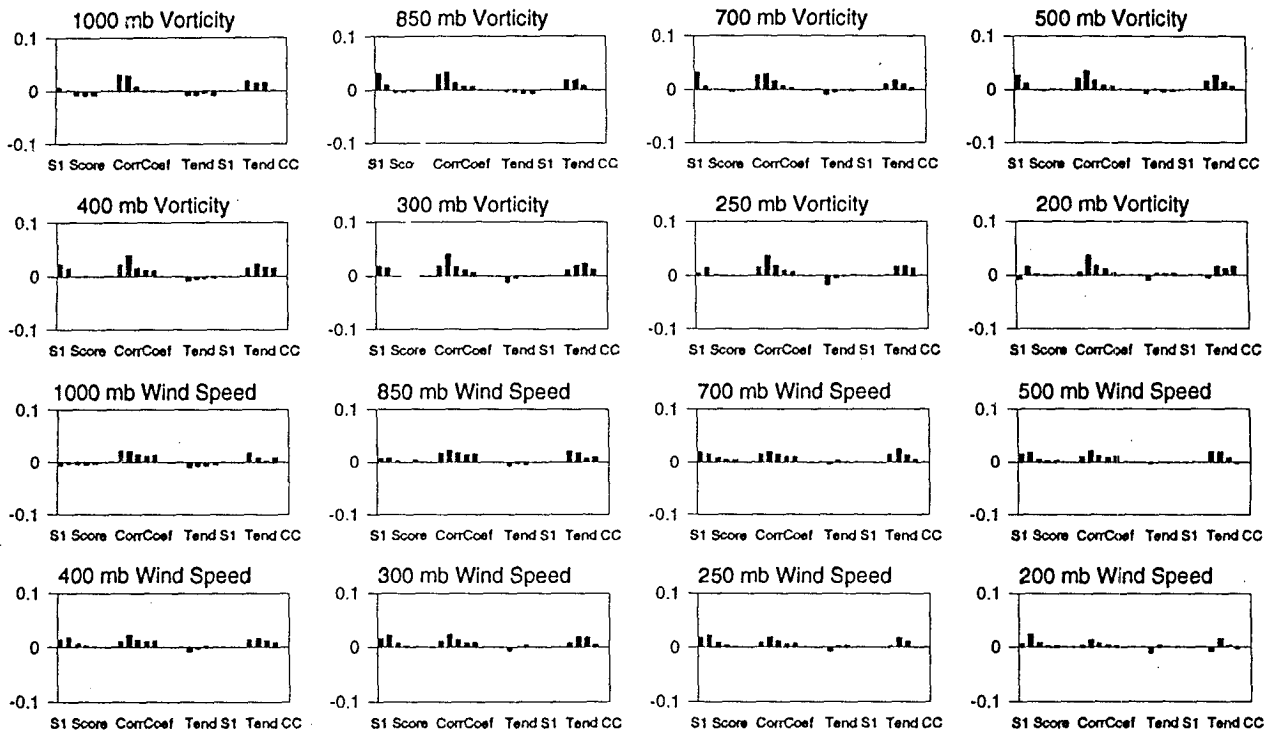## ETAY minus Early Eta

FIG. 12. Differences of the early eta and ETAY verification scores at the indicated pressure levels. At each pressure level: the differences are plotted for 00-, 12-, 24-, 36-, and 48-h forecasts (left to right within each score); for S1 score correlation coefficient, tendency S1 score, and tendency correlation coefficient (left to right within each variable); for height, temperature, vorticity, and wind speed. Positive numbers indicate a better score for the ETAY versus the early eta system.

maxima, as shown in the original model terrain (OLD) and terrain difference field (OLD–NEW) for the eastern and western United States in Fig. 9. The greatest impact is seen in the western United States adjacent to terrain maxima (Sierra Nevada range, Colorado, Wasatch range near Salt Lake City), with elevations lowered by as much as 350 m. Smaller but still significant changes in model elevation are seen in the eastern United States, with the model terrain in northern Virginia near IAD lowered by 25–75 m.

b. Analysis changes

In addition to the new model terrain specification, a series of changes to the eta ROI analysis algorithm were made, as summarized below.

1) The OI analysis is now performed directly on the eta model grid, thus eliminating the latitude–longitude analysis grid and interpolation errors between the two grids.

2) Observations that have a surface pressure up to 25 mb *greater* than the surface pressure of the model terrain are included in the analysis.

3) To better couple the surface observations with the lowest model layer, a 10-mb thick "mini-profile" is constructed from the surface observation, where the surface virtual temperature increment is used to produce a thickness increment.

4) The coefficients that define the width of the horizontal (k_h) and vertical (k_p) forecast error correlation functions for mass, wind, and moisture were increased, with the largest increase in the lowest model layers [Table 2; compare to Table 1 in DiMego (1988)]. The impact of this change in the OI algorithm is to give more weight to observations in closer proximity to the analysis grid point than was done previously. In the original early eta OI algorithm, the values of k_h in Table 2 were not adjusted for the location of the surface, an error that was changed in the ETAY system. In the original formulation, if the surface was located on analysis level 4, the OI algorithm would use $k_h = 3.325 \times 10^{-6}$ km^{-2}. In the ETAY system, the OI algorithm will use the value intended for the lowest analysis level, $k_h = 7.391 \times 10^{-6}$ km^{-2}. The analysis on level 5 would now employ the value intended for the second layer
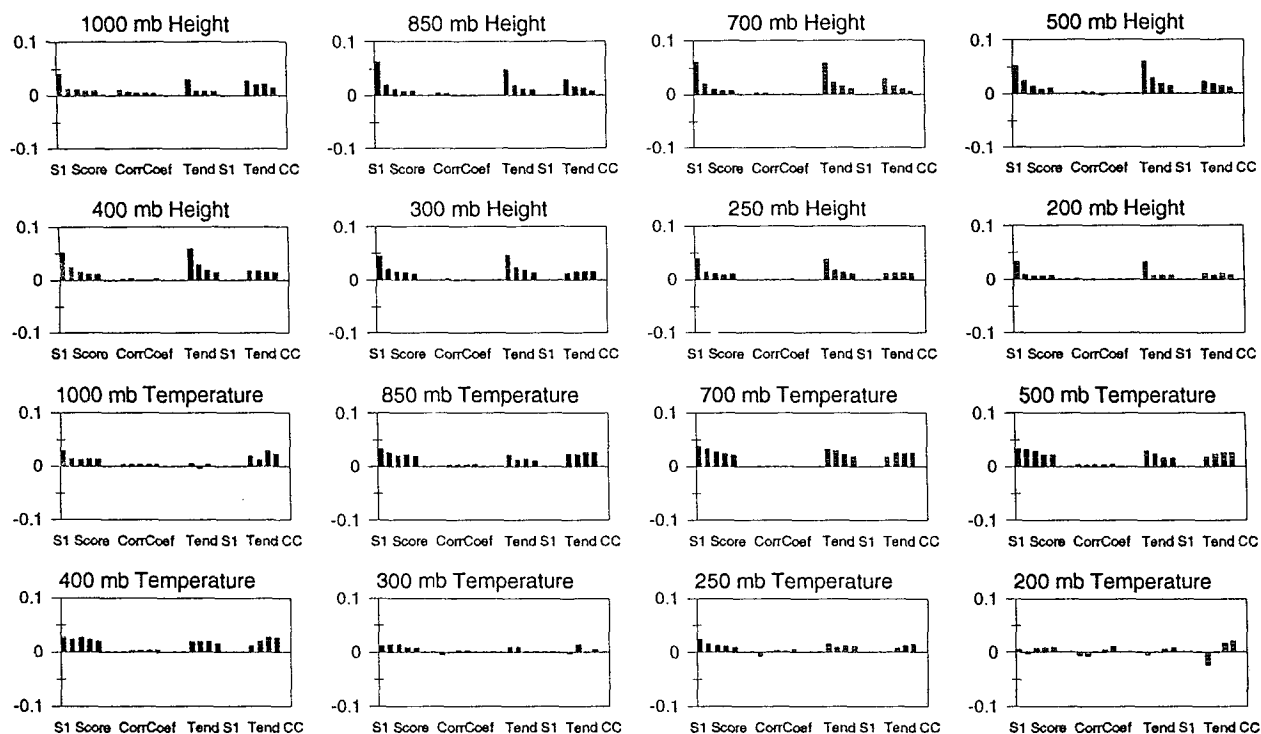
Verification Score Differences
ETAY minus Early Eta

FIG. 12. (Continued)

above ground, $k_h = 6.775 \times 10^{-6}$ km^{-2}, instead of k_h = 3.080 $\times$ 10^{-6} km^{-2}, and so on up to the fifth level above ground, after which the numbers in Table 2 are used directly.

5) The geostrophic coupling of wind increments with height increments was increased in all but the four bottom model layers. This change retains the frictional effects in the lowest layers but increases the influence of wind increments on the geopotential height analysis (and visa versa) in the middle and upper troposphere. The adjustment applied in item 4 above was also applied to the coefficients that control geostrophic coupling of the increments.

c. Impact—1200 UTC 9 February 1994 case

The impact of these changes are apparent in the stations selected for the lowest model layer height analysis near IAD (Fig. 10) using the new terrain and analysis package. Unlike the early eta analysis (Fig. 8), the ETAY analysis used both the DCA and IAD observations. Those stations located at a considerable distance from IAD were given less weight than in the early eta analysis. The post-processed 2-m temperature from

the 1200 UTC 9 February 1994 ETAY analysis (Fig. 11) is about 1°–2°C cooler than the early eta analysis over northern Virginia, although the cool pool over central Maryland is not depicted in the ETAY analysis. With 38 vertical layers, the eta ROI analysis should have sufficient vertical resolution to resolve shallow features, such as cold-air damming events. However, the lower-resolution first guess from the GDAS (T126, 28 layers) may not have been able to capture the feature in enough detail. Given the minor improvement in analyzed shelter temperature seen in the ETAY analysis, it appears that the changes tested in the ETAY system, while positive, are insufficient to capture the details of the low-level temperature field in this case.

d. Objective verification—May 1994

The verification score differences between the early eta and the ETAY for height, temperature, wind speed, and vorticity are shown in Fig. 12, with the RAFS analysis used for verification. These scores are identical to those computed for the early eta–LFM comparison (Black et al. 1993) discussed in section 4a. A positive difference indicates a higher score or correlation coef-
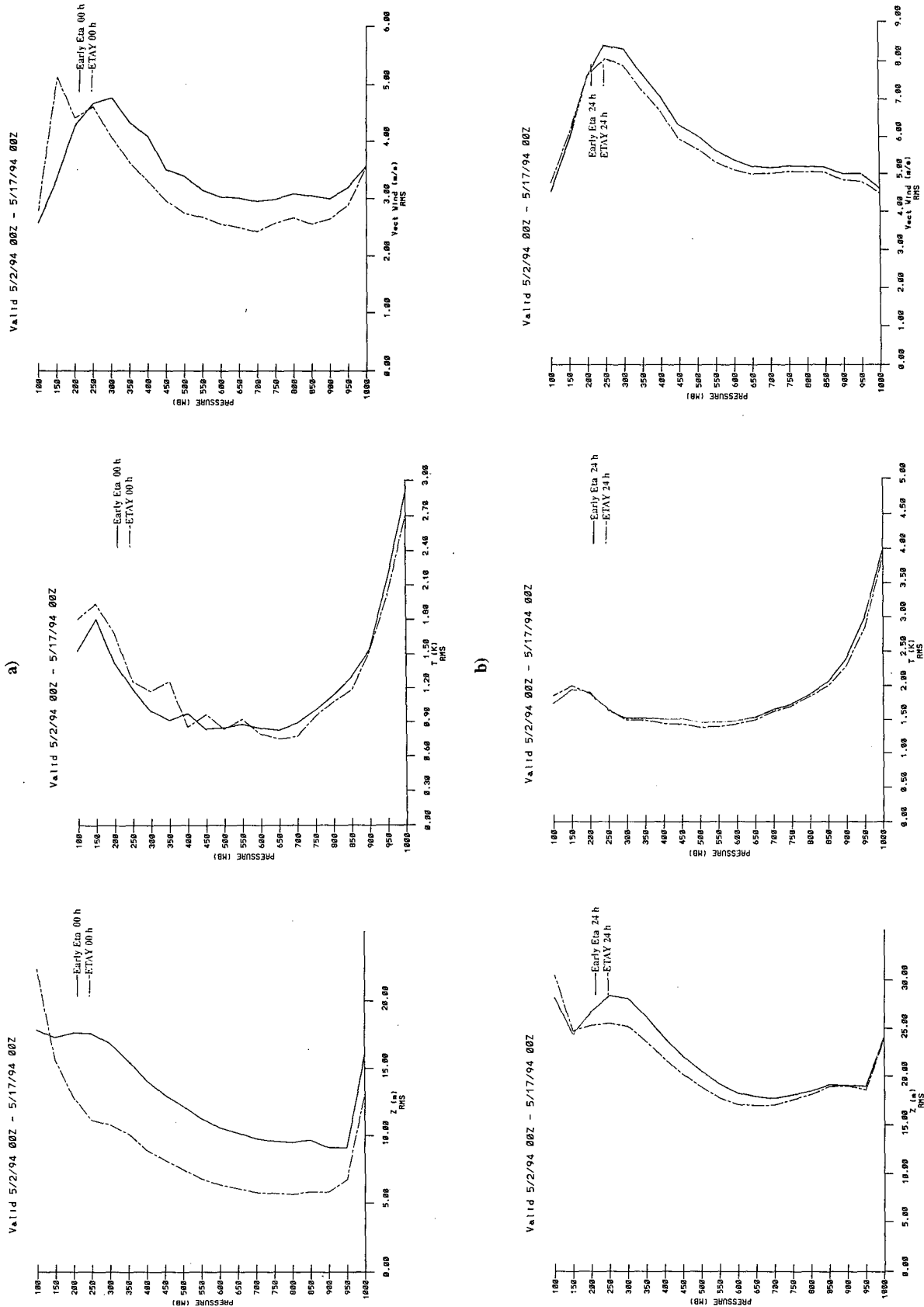
FIG. 13. Forecast versus rawinsonde root-mean-square errors for the (a) 00-h and (b) 24-h early eta (solid) and ETAY (dashed) forecasts of height, temperature, and vector wind for the period 2–17 May 1994.

Equitable Threat – All Periods
Valid 4 May 94 – 18 May 94

⊕ Early Eta
□ ETAY

EQ THREAT

0.6

0.4

0.2

0.0

| 0.01 | 0.10 | 0.25 | 0.50 | 0.75 | 1.00 | 1.50 | 2.00 |
| 15831 | 9425 | 5193 | 2408 | 1244 | 643 | 191 | 66 |

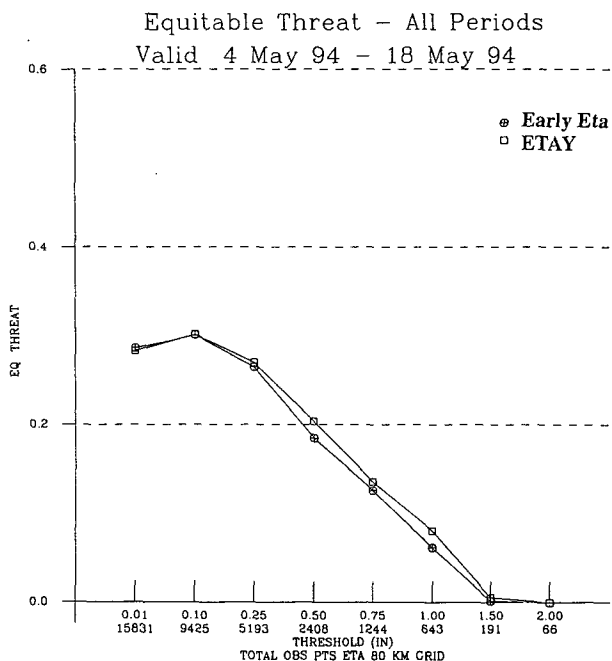THRESHOLD (IN)
TOTAL OBS PTS ETA 80 KM GRID

FIG. 14. Equitable threat skill scores for precipitation forecasts (all periods) from the early eta and ETAY systems for 4–18 May 1994.

ficient for the ETAY. Figure 12 demonstrates that the ETAY scores are better then the early eta scores in the vast majority of comparisons.

The analysis and 24-h forecast early eta–ETAY versus rawinsonde rms error scores for height, temperature, and vector wind are presented in Fig. 13. Only rawinsondes over the contiguous United States were used. The analysis height data shows that the combined analysis–terrain changes in the ETAY runs resulted in reduced rms errors at all levels below 100 mb, while the analysis vector wind and temperature scores from the ETAY are better in the lower and midtroposphere but slightly higher than the early eta in the upper troposphere. In general, the analysis patterns in the fit to the rawinsondes was carried over into the 24-h forecasts, although the rms error differences between the ETAY and early eta were reduced. Since the primary source of high density upper-level wind information is from aircraft data, it appears that the strengthened geostrophic coupling of the wind and height increments in the ETAY test had the anticipated effect of improving the wind analysis and favorably affecting the geopotential height analysis. The trend toward lower rms errors in the ETAY analysis also extended below 850 mb, indicating the positive effects of the treatment of the surface in the ETAY analysis. The reasons for the slight worsening of the ETAY analysis fit to the rawinsonde temperature and wind data in the middle and upper troposphere are not clear, but it is possible that the geostrophic coupling of height–wind increments is in need of further adjusting in the ROI algorithm.

Nonetheless, the improvement in the fit of the 24-h forecasts to the rawinsonde data in the ETAY system shows that the analysis–terrain changes were beneficial.

The precipitation ETS for 4–18 May 1994 (Fig. 14) reveals that the ETAY was incrementally better than the early eta for all forecast periods and thresholds except at the rain–no-rain threshold, where the early eta was slightly better. The bias statistics for the same period (Fig. 15) show a marginal decrease in the ETAY bias score versus the early eta forecast, especially at thresholds above 0.5 inches.

6. The Eta Data Assimilation System

Although the changes to the early eta system as described in section 5 produced incremental improvement in analysis and model performance, the early eta versus RAFS grid to observation verification comparison shown in Fig. 3 suggests that the use of a regional data assimilation system is important to produce analyses which more closely fit the observations. If the regional system has more frequent analysis updates (≤ 3 h), it will be able to assimilate high frequency observations (such as wind profilers) in a more timely manner than a global model-based system like the GDAS, which uses a 6-h analysis update cycle.

The NCEP has developed the Eta Data Assimilation System (EDAS), which is analogous to the intermittent Regional Data Assimilation System (RDAS: DiMego et al. 1992) used to initialize the NGM. The chart shown in Fig. 16 compares the analysis cycle in the original early eta system and one using the EDAS. The
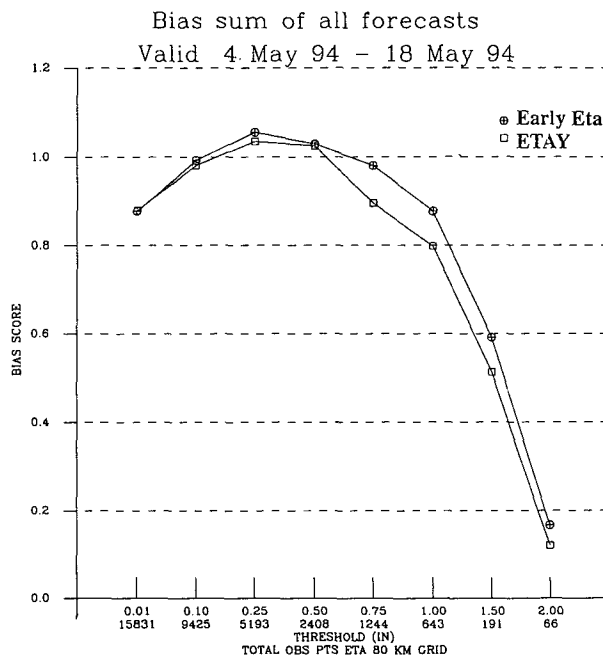
Bias sum of all forecasts
Valid 4 May 94 – 18 May 94

⊕ Early Eta
□ ETAY

BIAS SCORE

1.2

1.0

0.8

0.6

0.4

0.2

0.0

| 0.01 | 0.10 | 0.25 | 0.50 | 0.75 | 1.00 | 1.50 | 2.00 |
| 15831 | 9425 | 5193 | 2408 | 1244 | 643 | 191 | 66 |

THRESHOLD (IN)
TOTAL OBS PTS ETA 80 KM GRID

FIG. 15. Same as Fig. 14 but for bias scores.

OPERATIONAL 80 KM "EARLY" ETA

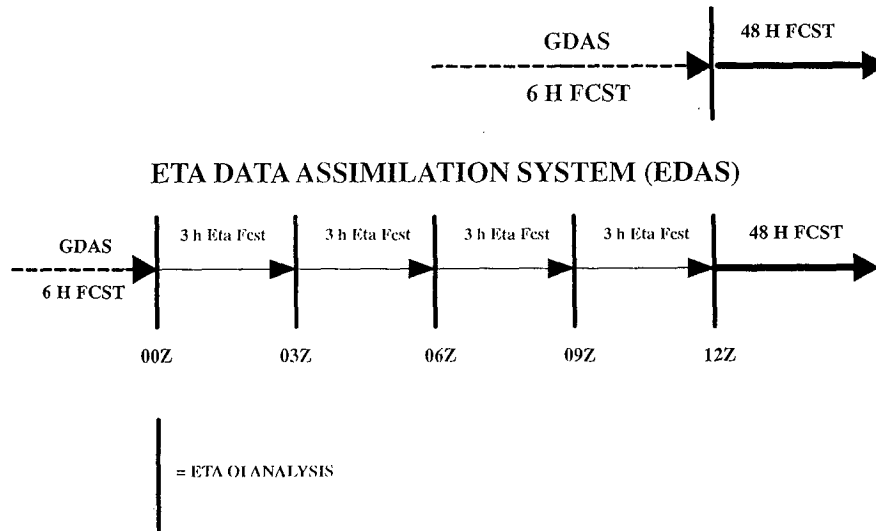ETA DATA ASSIMILATION SYSTEM (EDAS)

FIG. 16. Schematic comparison of the static OI analysis used in the original early eta system
and the intermittent eta data assimilation system.

EDAS consists of a series of 3-h analysis–forecast cycles, initiated using a 6-h forecast from the GDAS. The 3-h analysis updates are repeated until an analysis is obtained from which a 48-h eta model forecast can be started. As in the RDAS, the 3-h analysis updates allow for the use of high frequency observations such as aircraft data in a more timely manner than the GDAS. The use of the a regional or mesoscale model during the assimilation will produce a more consistent first guess and helps in improving skill in forecasting precipitation (Rogers et al. 1995).

1200 UTC 9 February 1994 case

The ability of the EDAS to improve eta model initial conditions is evident from the two analyses valid at 1200 UTC 9 February 1994, depicted in Fig. 17. These EDAS analyses, performed at 80 and 29 km, respectively, were produced using the 12-h data assimilation cycle depicted in Fig. 16. The 2-m temperature from the 80-km EDAS analysis is a considerable improvement over both the early eta (Fig. 7) and ETAY analyses (Fig. 11). Instead of the west–east-oriented temperature field in the static analyses, the 80-km EDAS was able to capture the cooler air over central Maryland, northern Virginia, and eastern Pennsylvania. The 80-km EDAS failed to reproduce the southern extension of the cooler air into southeastern Virginia. The analysis produced by a 29-km EDAS extended the cooler air farther south along the Virginia coast but produced temperatures $4°-6°C$ too low over the Washington, D.C. area.

Since the 29-km EDAS described above used the same analysis parameters as the 80-km EDAS, it

seemed prudent to attempt an experiment with the 29-km EDAS in which the analysis parameters were tuned to account for the higher-resolution analysis. In this test, the horizontal correlation factors in the ROI algorithm were increased by a factor of two above the 80-km values used in the ETAY and 80-km EDAS analyses. The analysis employing this change (Fig. 18) increased the temperatures near IAD to $-3°C$, still too low but an improvement over the control 29-km EDAS and much closer to the observed pattern than the early eta and ETAY analyses. While this sharpening of the correlations was a one-time test not supported by any longer-term statistical evidence, it does show that the eta OI analysis can be tuned to produce improved mesoscale analyses.

7. Summary

The OI analysis package used to create initial conditions for the NCEP operational "early" eta model has been described. Although the quantitative statistics show that the eta model is superior to the LFM (Black et al. 1993) and produces better precipitation forecasts than the NGM, deficiencies were found in the analysis component of the operational eta system, especially in the treatment of surface observations and in the model orography algorithm. Changes to alleviate these problems led to a better definition of the model orography and a more realistic treatment of surface data. These changes generally produced small positive impact on model performance during parallel testing, with the greatest impact observed in the analysis of low-level parameters. Based on these findings, these changes were

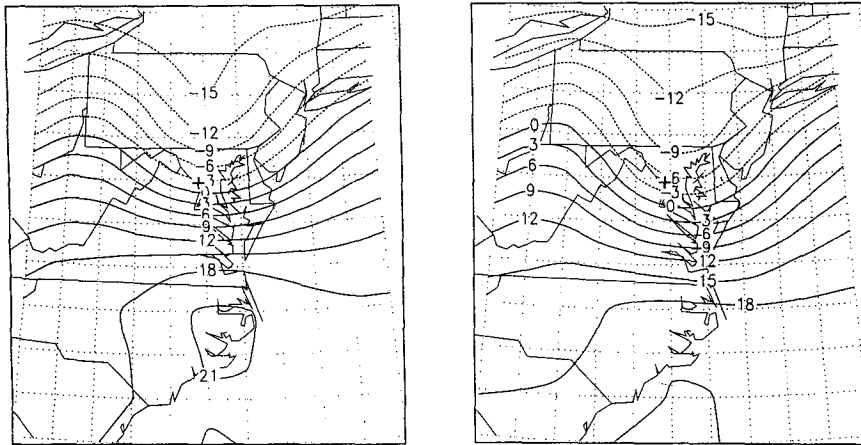a) 80 KM EDAS   b) 29 KM EDAS

FIG. 17. Same as Fig. 7 but from (a) the 80-km EDAS analysis and (b) the 29-km EDAS analysis valid 1200 UTC 9 February 1994.

implemented into the operational early eta model at 1200 UTC 7 September 1994.

The NCEP is now undertaking accelerated development of a mesoscale version of the eta model (Black 1994), concurrently with the development of a mesoscale eta-based intermittent data-assimilation system. The mesoscale eta model incorporates recent enhance-

FIG. 18. Same as Fig. 17 but from the 29-km EDAS analysis with enhanced horizontal correlation factors for wind, height, and specific humidity.

ments of the model physics, such as the use of an explicit cloud prediction scheme (Zhao and Black 1994). The purpose of this work is to produce operational mesoscale forecasts over the contiguous United States, initially twice a day and perhaps increased to four times a day by late 1995 or 1996. Toward that end, the NCEP has performed twice-daily experimental forecasts of the mesoscale eta model at 29-km grid over the contiguous United States with 50 vertical levels since April 1995. Initial conditions for this run are obtained from a 3-h "mini" EDAS initiated at 0000–1200 UTC from a GDAS first guess. The 3-h forecast from 0000–1200 UTC is used as background for the 0300–1500 UTC eta OI analysis, data for which will be obtained primarily from surface, wind profiler, and aircraft reports. After the 0300–1500 UTC analysis is completed, a 33-h mesoscale eta forecast is performed. After the evaluation of the performance of the mesoscale eta model performed during the spring of 1995, the mesoscale eta model and data assimilation system was operationally implemented at the NCEP in August 1995. The NCEP note describing the operational mesoscale eta system in detail will be published in the near future in this journal.

In addition to the mesoscale eta system, the NCEP has incorporated all the analysis–model enhancements developed for the mesoscale version into the early eta system. This upgrade allows the NCEP to improve early eta guidance for operational forecasters and simplifies eta model maintenance. Since the NCEP is committed to providing mesoscale forecasts for Alaska (which is outside of the 29-km eta model domain), an increase in resolution has accompanied the upgrade of the version of the model used in the early eta system. This upgrade, operationally implemented in September 1995, consists of three major components:
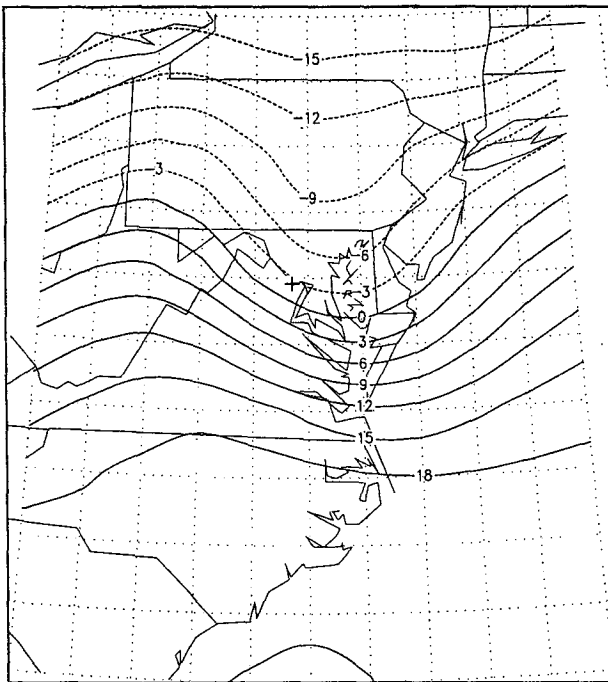
1) an increase in horizontal resolution from 80 to 48 km (number of vertical levels will remain set to 38);

2) all improvements to the eta model physical package (e.g., the cloud prediction scheme) developed for the mesoscale eta model are used;

3) a 12-h EDAS cycle with 3-h analysis updates at 48-km resolution replaces the static OI analysis used to provide initial conditions to the early eta model.

A description of each upgrade component, along with the impact of the full upgrade package on early eta performance (Rogers et al. 1995) will be the subject of an upcoming NCEP note in this journal.

APPENDIX

Definition of Objective Verification Scores

a. Precipitation: Equitable threat score and bias score

The equitable threat score (ETS) and bias score are defined as

$$\text{ETS} = \frac{H - CH}{F + O - H - CH} \quad \text{Bias} = \frac{F}{O}, \quad (A1)$$

where F is the number of forecast points above a threshold, O is the number of observed points above a threshold, H is the number of hits above a threshold, and CH is the expected number of hits in a random forecast of F points for O observed points, which is equal to

$$CH = \frac{F \times O}{\text{NUM}}, \quad (A2)$$

where NUM is the number of points in the verification domain. Whereas the simple threat score is the quotient of the intersection of the observed and forecast areas

of precipitation ("hits") divided by the union of these areas, the equations for ETS replaces the number of hits in the original formulation with the number of hits above the expected number when forecasting at random. The ETS has a similar range and interpretation as the simple threat score (ETS = 1 for a perfect forecast).

b. Grid to station verification scores

The S1 score (Teweles and Wobus 1954) verifies forecast gradients of a field against the observed gradients of the field. Here S1 is expressed as

$$\text{S1} = 100 \frac{|\text{ERR}|}{|\text{GRAD}|}, \quad (A3)$$

where $|\text{ERR}|$ is the sum of the magnitudes of the forecast error in the gradient component in each direction and $|\text{GRAD}|$ is the sum of the magnitudes of either the forecast or observed gradient component, whichever is larger. Although normally expressed in percent (%), we choose to express S1 as

$$\text{S1} = 1 - \frac{|\text{ERR}|}{|\text{GRAD}|}. \quad (A4)$$

Term S1 will then have a similar range (1.0–0.0) and interpretation (1.0 = perfect forecast) as a correlation coefficient.

The field correlation coefficient is the correlation of the forecast with the verifying analyses. The tendency correlation coefficient correlates the 12-h forecast change with the observed change. The tendency S1 score verifies gradients in the 12-h change field. For these four scores a perfect forecast would achieve a score of 1; therefore, a bigger score is better.

REFERENCES

Arakawa, A., and V. R. Lamb, 1977: Computational design of the basic dynamical processes of the UCLA general circulation model. *Methods in Computational Physics,* Vol. 17, Academic Press, 173–265.

Betts, A. K., and M. T. Miller, 1986: A new convective adjustment scheme. Part II: Single column tests using GATE wave, BOMEX, and arctic air-mass data sets. *Quart. J. Roy. Meteor. Soc.,* **112,** 693–709.

Black, T. L., 1988: The step-mountain eta coordinate regional model: A documentation. NOAA/NWS/NMC, 47 pp. [Available from National Meteorological Center, NOAA Science Center, 5200 Auth Road, Camp Springs, MD 20746.]

——, 1994: The new NMC mesoscale eta model: Description and forecast examples. *Wea. Forecasting,* **9,** 265–278.

——, D. G. Deaven, and G. J. DiMego, 1993: The step-mountain eta-coordinate model: 80 km 'Early' version and objective verifications. Technical Procedures Bulletin 412. NOAA/NWS, 31 pp. [Available from National Weather Service, Office of Meteorology, 1325 East-West Highway, Silver Spring, MD 20910.]

Collins, W. G., and L. S. Gandin, 1992: Complex quality control of rawinsonde height and temperatures at the National Meteorological Center. NMC Office Note 390, 166 pp. [Available from Development Division, National Meteorological Center, WWB Room 204, 5200 Auth Road, Camp Springs, MD 20746.]

DiMego, G. J., 1988: The National Meteorological Center Regional Analysis System. *Mon. Wea. Rev.,* **116,** 977–1000.

——, and Coauthors, 1992: Changes to NMC's Regional Analysis and Forecast System. *Wea. Forecasting,* **7,** 185–198.

Fels, S. B., and M. D. Schwarztkopf, 1975: The simplified exchange approximation: A new method for radiative transfer calculations. *J. Atmos. Sci.,* **32,** 1475–1488.

Gandin, L. S., L. L. Morone, and W. G. Collins, 1993: Two years of operational comprehensive hydrostatic quality control at the National Meteorological Center. *Wea. Forecasting,* **8,** 57–72.

Gerrity, J. P., Jr., T. L. Black, and R. F. Treadon, 1994: The numerical solution of the Mellor–Yamada 2.5 turbulent kinetic energy equation in the eta model. *Mon. Wea. Rev.,* **122,** 1640–1646.

Hoke, J. E., N. A. Phillips, G. J. DiMego, J. J. Tuccillo, and J. G. Sela, 1989: The Regional Analysis and Forecast System of the National Meteorological Center. *Wea. Forecasting,* **4,** 323–334.

Janjic, Z. I., 1990: The step mountain coordinate: Physical package. *Mon. Wea. Rev.,* **118,** 1429–1443.

——, 1994: The step-mountain eta coordinate model: Further developments of the convection, viscous sublayer, and turbulence closure schemes. *Mon. Wea. Rev.,* **122,** 927–945.

Joseph, D., 1980: Navy 10 minute global elevation values. National Center for Atmospheric Research Notes on Fleet Numerical Weather Center Terrain Data Set, 3 pp. [Available from the National Center for Atmospheric Research, P.O. Box 3000, Boulder, CO 80307.]

Kanamitsu, M., and Coauthors, 1991: Recent changes implemented into the Global Forecast System. *Wea. Forecasting,* **6,** 425–435.

Lacis, A. A., and J. E. Hansen, 1974: A parameterization of the absorption of solar radiation in the earth's atmosphere. *J. Atmos. Sci.,* **31,** 118–133.

Liu, W. T., K. B. Katsaros, and J. B. Businger, 1979: Bulk parameterizations of air–sea exchanges of heat and water vapor including the molecular constraints at the interface. *J. Atmos. Sci.,* **36,** 1722–1735.

Mangarella, P. A., A. J. Chambers, R. L. Street, and E. Y. Hsu, 1973: Laboratory studies of evaporation and energy transfer through a wavy air–water interface. *J. Phys. Oceanogr.,* **3,** 93–101.

Mellor, G. L., and T. Yamada, 1974: A hierarchy of turbulence closure models for planetary boundary layers. *J. Atmos. Sci.,* **31,** 1791–1806.

——, and ——, 1982: Development of a turbulence closure model for geophysical fluid problems. *Rev. Geophys., Space Phys.,* **20,** 851–875.

Mesinger, F., 1984: A blocking technique for representation of mountains in atmospheric models. *Riv. Meteor. Aeronaut.,* **44,** 195–202.

——, and W. G. Collins, 1987: Review of the representation of mountains in numerical weather prediction models. *Observation, Theory, and Modeling of Orographic Effects, Seminar Notes,* Vol. 2. ECMWF, 1–28.

——, and T. L. Black, 1992: On the impact of forecast accuracy of the step-mountain (eta) vs. sigma coordinate. *Meteor. Atmos. Phys.,* **50,** 47–60.

——, S. Nickovic, D. Gavrilov, and D. G. Deaven, 1988: The step-mountain coordinate: Model description and performance for cases of Alpine lee cyclogenesis and a case of Appalachian redevelopment. *Mon. Wea. Rev.,* **116,** 1493–1518.

——, T. L. Black, and M. E. Baldwin, 1995: Impact of resolution and of the eta coordinate on skill of the eta model precipitation forecasts. *Atmos.-Ocean.,* in press.

Rogers, E., T. L. Black, D. G. Deaven, G. J. DiMego, Q. Zhao, Y. Lin, N. W. Junker, and M. E. Baldwin, 1995: Changes to the NMC operational eta model analysis/forecast system. Technical Procedures Bulletin #423, NOAA/NWS, 60 pp. [Available from National Weather Service, Office of Meteorology, 1325 East-West Highway, Silver Spring, MD 20910.]

Schaefer, J. T., 1990: The critical success index as an indicator of warning skill. *Wea. Forecasting,* **5,** 570–575.

Teweles, S., and H. Wobus, 1954: Verification of prognostic charts. *Bull. Amer. Meteor. Soc.,* **35,** 455–463.

Woollen, J. S., 1991: New NMC operational OI quality control. Preprints, *Ninth Conf. on Numerical Weather Prediction,* Denver, CO, Amer. Meteor. Soc., 24–27.

Zhao, Q., and T. L. Black, 1994: Implementation of the cloud scheme in the eta model at NMC. Preprints, *10th Conf. on Numerical Weather Prediction,* Portland, OR, Amer. Meteor. Soc., 331–332.